Investigation of a Nanocomposite of 75 wt % Poly(methyl methacrylate) Nanoparticles with 25 wt % Poly(ethylene oxide) Linear Chains: A Quasielatic Neutron Scattering, Calorimetric,...

ARTICLE *in* MACROMOLECULES · MAY 2014

Impact Factor: 5.8 · DOI: 10.1021/ma500215f

Macromolecules

Article

pubs.acs.org/Macromolecules

Investigation of a Nanocomposite of 75 wt % Poly(methyl methacrylate) Nanoparticles with 25 wt % Poly(ethylene oxide) Linear Chains: A Quasielatic Neutron Scattering, Calorimetric, and WAXS Study

D. Bhowmik,[†] J. A. Pomposo,[‡,§,∥] F. Juranyi,[⊥] V. García Sakai,[#] M. Zamponi,[%] A. Arbe,*[,‡] and J. Colmenero[†,‡,§]

[†]Donostia International Physics Center, Paseo Manuel de Lardizabal 4, 20018 San Sebastián, Spain

[‡]Centro de Física de Materiales (CSIC−UPV/EHU) − Materials Physics Center (MPC), Paseo Manuel de Lardizabal 5, 20018 San Sebastián, Spain

[§]Departamento de Física de Materiales, UPV/EHU, Apartado 1072, 20080 San Sebastián, Spain

[∥]IKERBASQUE - Basque Foundation for Science, Alameda Urquijo 36, 48011 Bilbao, Spain

[⊥]Laboratory for Neutron Scattering, Paul Scherrer Institut, CH-5232 Villigen, Switzerland

[#]ISIS Facility, Rutherford Appleton Laboratory, Harwell Science & Innovation Campus, Chilton, Didcot OX11 0QX, United Kingdom

[%]Jülich Centre for Neutron Science, Forschungszentrum Jülich GmbH, outstation at Heinz Maier-Leibnitz Zentrum, Lichtenbergstr. 1, 85747 Garching, Germany

Supporting Information

ABSTRACT: We have investigated the thermal behavior, local structure, and dynamics in a system where 25 wt % PEO [poly(ethylene oxide)] linear chains are mixed with 75 wt % PMMA [poly(methyl methacrylate)] soft nanoparticles. Calorimetric and wide-angle X-ray scattering experiments point to a weak penetration of the PEO chains in the nanoparticles, qualifying the mixture as a nanocomposite. Quasi-elastic neutron scattering (QENS) experiments on partially deuterated samples has selectively revealed the component dynamics in the system. The α-methyl group dynamics of PMMA, which fall within the QENS time scale in the temperature range investigated, are hardly affected by the presence of PEO except for hints of a more heterogeneous environment in the nanocomposite than in bulk PMMA. The effects on the dynamics of PEO are more interesting. The observation of dynamics in the microseconds range for the PEO component of the nanocomposite at temperatures at which the calorimetric experiments indicate the freezing of its segmental relaxation provides evidence for confined dynamics below the main glass transition of the mixture—attributable to the effective glass transition of the slow component. A parallel study on an equivalent blend of PEO and linear PMMA chains shows that these effects are independent of the topology of the PMMA. However, well above the effective glass transition of the slow component, the dynamics of PEO differ in both systems. In the linear blend, PEO segments move with the typical features of supercooled polymers in metastable equilibrium, while in the nanocomposite PEO dynamics exhibit an anomalously strong deviation from Gaussian behavior. This deviation grows with increased mobility of the nanoparticles. PEO segments are seemingly trapped in effective cages imposed by the nanoparticles for a very long time—more than 2 orders of magnitude longer than in bulk or when surrounded by linear PMMA chains—before the subdiffusive process leading to segmental relaxation sets in. We speculate that local loops in the surface of the nanoparticles may play an important role in this trapping mechanism.

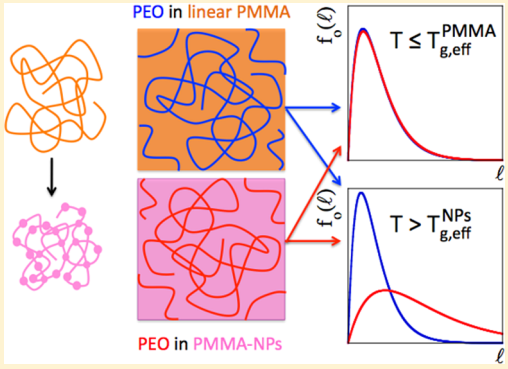

I. INTRODUCTION

Because of difficulties in commercializing new polymers, industry has turned increasingly to blending existing polymers to optimize their end-use (e.g., mechanical and rheological) properties. In particular, blends based on thermodynamically miscible polymers are one of the most efficient and economical means to create new materials with tailored features. An alternative route to tune polymer properties is via the addition of nanoparticles.

Received: January 28, 2014
Revised: April 23, 2014
Published: May 2, 2014

In this direction, the use of single-chain polymer nanoparticles ("soft" nanoparticles) seems to be particularly promising. Soft nanoparticles obtained by intramolecular cross-linking of linear macromolecules (precursors) are emerging soft nano-objects showing unique and remarkable physicochemical, rheological, and sensing properties due to their locally collapsed structure and ultrasmall size.[1−3] Intriguing nanoscale effects leading to strong reductions in melt viscosity, nanoparticle segregation to interfaces, and dewetting inhibition have been reported for binary nanocomposites composed of high-molecular-weight polymer-A and polymer-A soft nanoparticles (i.e., athermal all-polymer nanocomposites).[1,4,5] Nanocomposites consisting of linear polymers mixed with soft nanoparticles are in fact blends of polymers where one of the components is internally cross-linked.

The design of tailor-made materials would be greatly aided by an accurate understanding of the mixtures at a molecular level. Of particular impact for determining the end-use properties is the dynamic response of the material. Therefore, in both kinds of systems—blends of linear chains and nanocomposites of linear polymers and nanoparticles—a key question to address is, *how are the dynamics of each component modified by the presence of the other one?* In the case of linear blends a large effort has been made during the past decades to elucidate this problem (see, as general references, the reviews[6,7]). To answer such a question, the use of experimental techniques that are component-selective is mandatory. NMR on deuterium-labeled samples or dielectric spectroscopy when only one of the components is dielectrically active can be highly efficient methods. Quasi-elastic neutron scattering (QENS) combined with isotopic labeling is a technique of special interest since it also provides spatial information through the momentum transfer (Q) dependence of the measured magnitudes. From diverse investigations by different methods on thermodynamically miscible polymer blends, it has been concluded that blending does not essentially perturb the local dynamics relevant in the glassy state like methyl-group rotations or motions involved in secondary relaxations. Regarding the α-process directly related with the glass-transition phenomenon, one well-established feature is the dynamic heterogeneity, i.e., the observation of two different characteristic times for segmental relaxation, each of them corresponding to the dynamics of one component modified by blending. This dynamic heterogeneity implicitly leads to the existence of two different glass transitions T_g, one for each component, referred to as "effective glass transition", $T_{g,eff}$. The consequences of dynamic heterogeneity are expected to be more dramatic in blends of polymers with large difference in the homopolymer T_g values.

This is the case of binary mixtures of poly(ethylene oxide) (PEO) ($T_g^{PEO} \approx 220$ K) and poly(methyl methacrylate) (PMMA) ($T_g^{PMMA} \approx 400$ K). In fact, these blends have attracted great attention in the scientific community.[8−54] Because of crystallization at moderate contents of PEO, most investigations have focused on compositions rich in the PMMA component (about 80% in PMMA). We note that in such cases the glass transition feature accessed e.g. by calorimetry is largely dominated by the effective glass-transition of the PMMA component $T_{g,eff}^{PMMA}$. Interestingly enough, NMR experiments[10,12,20] revealed a strong decoupling between PEO and PMMA dynamics. QENS results on the PEO component pointed to a dramatically stretched relaxation dynamics which was accounted for by invoking very broad distributions of relaxation times with a temperature-dependent width.[24,28] These broad distributions in the dynamics of the fast component were interpreted[28] as a consequence of the nonequilibrium situation reached by this component in the vicinity of the effective $T_{g,eff}$ of the slow component in the blend (PMMA). There, the chain and segmental dynamics of the slow component (matrix) could be considered to be completely frozen on the time scale of the segmental motions of the fast component. In that situation, the motions of the fast component can be expected to be localized and rather heterogeneous. This scenario was corroborated by data on blends of PEO with other linear polymers with high T_g values. Hints for similar confinement effects were found by QENS on a PEO/poly(vinyl acetate) (PVAc, 20/80%), where the glass transition temperatures of the homopolymers differ by about 100 K ($T_g^{PVAc} = 314$ K).[55] In that work, a crossover in the behavior of PEO was found around 70 K above the calorimetric T_g of the blend: at high temperatures, PEO behaves like a "standard" glass-forming system in supercooled regime, whereas signatures of confined dynamics were observed when decreasing the temperature toward the average T_g of the blend. Similar findings were obtained from the viscoelastic and dielectric relaxation investigation of the blend PEO/PVAc[56] and from QENS on a blend of PEO with poly(ether sulfone) (PES) ($T_g^{PES} = 382$ K).[57]

In this contribution we now ask, what happens if the rigid component is not a linear macromolecule but a single-chain soft nanoparticle? What is the impact of internal cross-linking of the slow component on the confinement effects of the fast component? With these ideas in mind, here we have investigated a mixture consisting of 25 wt % PEO linear chains and 75 wt % PMMA nanoparticles (PMMA-NPs). The equivalent blend of linear PEO and PMMA chains has also been studied as reference. We have performed calorimetric measurements to characterize the effective glass transitions of the components in these mixtures. Wide-angle X-ray scattering (WAXS) has been used to investigate the short-range order in the samples. One of the posed questions was to estimate the degree of interpenetration between the two components, i.e., to discern whether the system can be considered as a "true" nanocomposite (weak or basically no penetration of PEO in the nanoparticles) or, on the contrary, it would be more similar to a semi-interpenetrating network in which cross-linked PMMA is blended with PEO. Our experiments suggest the picture of a "true" nanocomposite as the most suitable one for the PEO/nanoparticles mixture. To disentangle the component dynamics at molecular level, QENS experiments were performed on selectively labeled (H/D) samples. The PMMA-NPs were deuterated in order to minimize their contribution to the scattered intensity and such that the recorded signal reveals the incoherent scattering function (self-motions) of the protons in PEO in the angstroms to nanometers length scale. Furthermore, we consider the effects of the presence of PEO on the dynamics of the nanoparticles by measuring an oppositely labeled system, deuterated PEO and protonated NP's.

II. EXPERIMENTAL SECTION

A. Samples. The nanoparticles were obtained through Michael addition-mediated multidirectional self-assembly of individual polymeric chains (precursors) at room temperature in tetrahydrofuran, by following the procedure reported in ref 58. As precursors, linear copolymers of methyl methacrylate (MMA) and (2-acetoacetoxy)ethyl methacrylate (AEMA) P($MMA_{0.65}$-*co*-$AEMA_{0.35}$) were used. To obtain the deuterated nanoparticles, the copolymer precursor was synthesized starting from deuterated MMA monomers. Ethylene glycol diacrylate (EGDA) (90%, Sigma-Aldrich) acted as intrachain cross-linking agent in all cases. A schematic diagram of the synthesis process is depicted in Figure 1. The kinetics corresponding to the consumption of cross-linker units (x) was followed by ^{1}H NMR measurements, revealing a value of

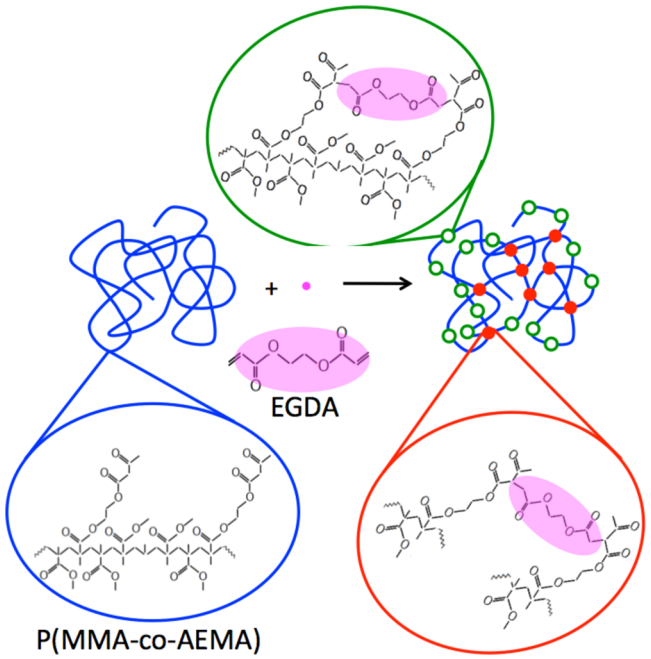

Figure 1. Schematic illustration of PMMA-NP synthesis through Michael addition-mediated multidirectional self-assembly using random copolymers of MMA and AEMA and EGDA as the intrachain cross-linking agent. The scheme shows the chemical composition of the P(MMA-*co*-AEMA) precursor and EGDA on the left. On the right is a representation of the two possible linkages resulting from the cross-linking process: connecting monomers located at a large contour distance along the chain (filled circles, lower panel) and bonding of nearest monomers along the chain (open circles, upper panel).

7.4×10^{-3} h^{-1} for the apparent rate k_{app} involved in the reaction $[x(t)] = [x(t = 0)] \exp(-k_{app}t)$.[58] Taking into account that the cross-linking reaction time was t_R = 72 h, the reacted fraction $c = 1 - ([x(t_R)]/[x(t = 0)])$ was about 0.4. From dynamic light scattering in dilute solution, the average hydrodynamic radii of the resulting nanoparticles were determined to be 7.4 ± 1.5 nm for the protonated samples and 8.1 ± 1.5 nm for the deuterated ones. Thus, both kinds of nanoparticles can be considered to be comparable in size. Two nanocomposites containing 25 wt % PEO and 75 wt % PMMA-NPs were prepared (*d*PEO/*h*NPs and *h*PEO/*d*NPs, respectively, where *d* stands for deuterated and *h* for protonated) by mixing appropriate amounts of deuterated PEO (*d*PEO, M_w = 89 kDa, M_w/M_n = 1.08, Polymer Source, Inc.) and protonated PMMA-NPs (*h*NPs, M_w = 72 kDa, M_w/M_n = 1.1) as well as protonated PEO (*h*PEO, M_w = 94 kDa, M_w/M_n = 1.08, Sigma-Aldrich) and deuterated PMMA-NPs (*d*NPs, M_w = 71 kDa, M_w/M_n = 1.1). The *d*PEO/*h*NPs and *h*PEO/*d*NPs mixtures were dissolved in chloroform and further precipitated in methanol. The resulting *d*PEO/*h*NPs and *h*PEO/*d*NPs blends were dried at 80 °C under dynamic vacuum until constant weight. The QENS samples were prepared by pressing the dried *d*PEO/*h*NPs and *h*PEO/*d*NPs systems in a hot-plate hydraulic press (Labopress 200-T, VOGT). For the reference blend (also 25% PEO/75% PMMA in weight), we used linear *h*PEO of M_w = 25 kDa and M_w/M_n = 1.03 and *d*PMMA of M_w = 27 kDa and M_w/M_n = 1.04. We will refer to this sample as *h*PEO/*d*PMMA.

B. Sample Characterization: Differential Scanning Calorimetry and WAXS. A differential scanning calorimeter TA Instruments Q2000 was used to measure the calorimetric glass transition temperature of the samples. Modulated differential scanning calorimetry (MDSC) allows to separate changes in the heat flow due to variations in the heat capacity (C_p) of the sample from other type of heat contributions, that is, the so-called reversible and nonreversible contributions. Samples of about 10 mg were sealed in aluminum pans and cooled at an average 3 K/min rate with temperature modulation amplitude and period of ±0.5 K and 60 s, respectively.

The static structure factor was investigated by WAXS on a Rigaku equipment with a two-dimensional multiwire X-ray Detector (Gabriel design, 2D-200X) of 200 mm diameter active area with ca. 200 μm resolution. The azimuthally averaged scattered intensities were obtained as a function of scattering vector $Q = 4\pi \sin(\theta)/\lambda$, where θ is half the scattering angle and λ = 1.54 Å from Cu K transition photons. Reciprocal space and absolute intensity calibrations were done using bromobenzoic acid and water, respectively, as standards. Measurements were performed in transmission geometry, with films fixed perpendicular to the beam (beam section: 1.3 mm) and at a distance of 24 cm from the detector. Using a Linkam Scientific Instruments THMS600 temperature controller, measurements were carried out at 100 °C on the mixtures and the pure components. For the *h*PEO/*d*PMMA blend and the *h*PEO/*d*NPs nanocomposite, the temperature dependence (from 200 to 400 K, every 10 K) of the static structure factor was also investigated.

C. QENS. Three different spectrometers were used to carry out the QENS measurements: the direct-geometry instrument FOCUS and the backscattering spectrometers IRIS and SPHERES. Table 1 summarizes the details of the instrumental conditions applied in each case. Combining the treated data, a wide window of correlation times (from the order of 10^{-13}–10^{-9} s) was covered. The determination of the resolution function $R(Q,\omega)$ was performed by measurements at 5 K. Flat aluminum cells were used as sample holder with a thickness adjusted for attaining close to 90% transmission. Empty sample holder signal was subtracted from the raw data followed by a correction of the detector efficiency. Measuring times of 2.5 h approximately were employed. The experiments were carried out every 25 K in the range 250 K ≤ T ≤ 400 K. As reference, the blend sample *h*PEO/*d*PMMA was measured on FOCUS in the same conditions in the temperature range 300 K ≤ T ≤ 400 K.

The QENS spectra were Fourier transformed and deconvoluted from the instrumental resolution, to obtain the intermediate scattering function in the time domain $I(Q,t)$ and to enable the merging of data from the different instruments. Details on this, on the models used for each sample, and on the assumptions made are fully described in section A of the Supporting Information.

III. RESULTS AND DISCUSSION

A. Determination of the Effective Glass Transitions. Complex materials like those here investigated may exhibit more than one single glass-transition process, associated with each of the components in the system. Sometimes it is not straightforward to distinguish the different vitrification phenomena from the inspection of the specific heat, which displays very broad features. In such cases, calculating the temperature derivative of this magnitude provides a sensitive method to disentangle the underlying glass transitions—the location of a maximum in this function corresponds to the inflection point in the specific heat which is associated with a given glass-transition process.

Table 1. Experimental Details of Different Spectrometers Used for QENS Measurements

spectrometer, facility	incident wavelength (λ) (Å)	wavevector (Q) range (Å^{-1})	energy transfer ($\hbar\omega$) range (meV)	energy resolution (fwhm) (μeV)	time range (s)
FOCUS, Paul Scherrer Institute	6.01	0.4–1.8	∼−1–500	∼42	$\sim10^{-13}$–10^{-11}
IRIS, ISIS Facility	6.65	0.5–1.8	∼−0.5–0.5	17.5	$\sim10^{-12}$–10^{-10}
SPHERES, FRM II	6.27	0.2–1.9	∼−0.031–0.031	0.65	$\sim10^{-10}$–10^{-9}

dx.doi.org/10.1021/ma500215f | *Macromolecules* 2014, 47, 3005−3016

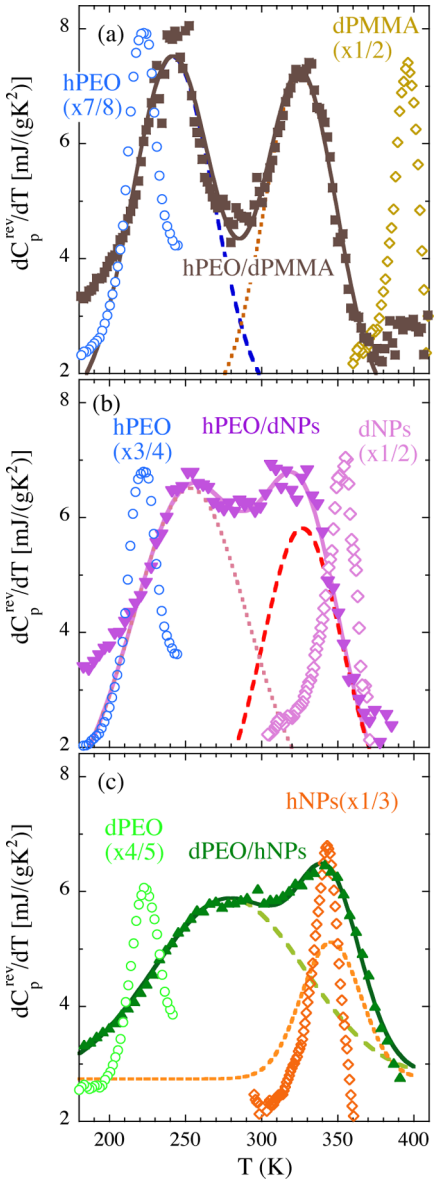

Figure 2. Temperature dependence of the derivative of the reversible heat flow with respect to temperature of the mixtures (filled symbols) and the pure components (circles: PEO; diamonds: PMMA or nanoparticles) for (a) blend of *h*PEO with linear *d*PMMA, (b) nanocomposite *h*PEO/*d*NPs, and (c) nanocomposite *d*PEO/*h*NPs. For clarity, the factors indicated have been applied to the data corresponding to the pure systems. Solid lines are fits of the sum of two Gaussians (depicted with the dashed and dotted lines) and a constant to the data of the mixtures.

The results obtained by this procedure are represented in Figure 2 for the linear blend (Figure 2a) and the two differently labeled PEO/NPs mixtures (Figure 2b,c). The figures also show the results on the respective pure components.

The data corresponding to the neat systems display a single clear glass-transition. Fits of a Gaussian $\propto \exp[-(T - T_g)^2/(2(\Delta T_g)^2)]$ to the peak—plus a flat background—deliver the value of the glass-transition temperature T_g and the width ΔT_g of these processes. They are collected in Table 2. We note that the glass transition of the nanoparticles is clearly shifted to lower temperatures (about 50 K) with respect to that in linear *d*PMMA. This effect should be attributed to the internal plasticization of PMMA produced by the AEMA monomers in the NPs.[59] Even

Table 2. Glass Transition Temperature and Width (Maximum Position and Variance of the Gaussian Fit of the Heat-Flow Derivative) of the Neat Systems and the Components Involved in the Mixtures (Other: PMMA, NPs)

sample	T_g (K)	ΔT_g (K)	$T_{g,eff}^{PEO}$ (K)	$\Delta T_{g,eff}^{PEO}$ (K)	$T_{g,eff}^{other}$ (K)	$\Delta T_{g,eff}^{other}$ (K)
*h*PEO	223	12				
*d*PEO	224	12				
*d*PMMA	395	7				
*d*NPs	352	10				
*h*NPs	342	9				
*h*PEO/*d*PMMA			242	27	326	24
*h*PEO/*d*NPs			253	37	327	26
*d*PEO/*h*NPs			279	50	346	20

so, there is still a huge difference between the T_g values of the two pure components in the PEO/NPs mixed systems ($T_g^{NPs} - T_g^{PEO} \approx 125$ K). Now considering the results on the mixtures, the presence of two distinct processes is evident not only in the linear blend—which had already been reported from previous studies[31] (see Figure 2a)—but also for the PEO/NPs mixtures (Figure 2b,c). The data can be well described assuming two Gaussian components, as shown in the figure. These functions would be attributed to the "effective glass transitions" of each of the components in the mixtures: that centered at lower temperatures corresponding to the glass transition of PEO in the system and that at higher temperature to the slow component. The parameters corresponding to the effective glass transition temperature and width of each component in the mixed systems are also listed in Table 2. Thus, the results reveal dynamic heterogeneity also for the PEO/NPs mixtures [$T_{g,eff}^{NPs} - T_{g,eff}^{PEO} \approx 70$ K, Figure 2b,c], though the processes are more separated from each other in the case of the linear blend [$T_{g,eff}^{dPMMA} - T_{g,eff}^{hPEO} = 84$ K, Figure 2a]. Interestingly enough, the value of the effective glass transition of the slow component in the blend and the PEO/NPs mixtures is practically the same—or even higher in the case of the *d*PEO/*h*NPs system—though the value of T_g in the bulk of linear chains is much higher than in the bulk of NPs. In other words, the large shift observed for the glass transition of the linear PMMA chains upon blending ($T_g^{dPMMA} - T_{g,eff}^{dPMMA} \approx 70$ K) is dramatically reduced in the case of the *h*PEO/*d*NPs mixture ($T_g^{dNPs} - T_{g,eff}^{dNPs} \approx 25$ K) or even vanishes, within the uncertainties, in the *d*PEO/*h*NPs system. Thus, a much weaker plasticization effect is observed for the slow component if it is present in the form of nanoparticles. This finding discards a high degree of penetration of PEO in the nanoparticles. A substantial interpenetration would be expected to lead to a significant shift in the glass-transition temperature of the slow component—like in the linear blend—which is not observed in the NPs. We note that at the same time the vitrification temperature of the PEO component varies in the mixtures with respect to that in bulk, ruling out a phase separation. The results thus suggest a distribution of the PEO chain segments at the interfaces between the nanoparticles. The broadening of the effective glass transition of the NPs would be due to their plasticization at their surfaces.

B. Local Structure. Figure 3 shows the WAXS results for the linear blend *h*PEO/*d*PMMA (Figure 3a) and the mixtures *h*PEO/*d*NPs (Figure 3b) and *d*PEO/*h*NPs (Figure 3c). The data obtained for the respective homopolymers are included in each panel. The measurements correspond to 100 °C, where PEO is molten, for a meaningful comparison. In the *Q*-range explored, the patterns reveal broad peaks of the structure factor.

dx.doi.org/10.1021/ma500215f | *Macromolecules* 2014, 47, 3005−3016

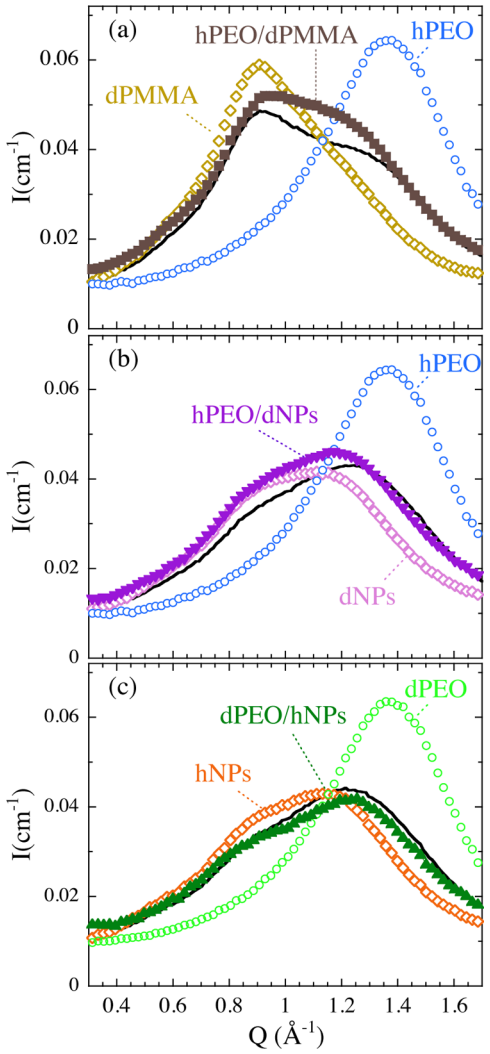

Figure 3. WAXS patterns obtained at 100 °C for PEO (empty circles), the other neat component (empty diamonds), and their mixtures: (a) Blend of *h*PEO and linear *d*PMMA (filled squares). (b) Nanocomposite of *h*PEO and *d*NPs (filled inverted triangles). (c) Nanocomposite of *d*PEO and *h*NPs (filled triangles). Solid lines represent the result of combining the patterns corresponding to the neat components weighed by the respective volume fractions in the mixtures $[I^{total}(Q) = \phi^{PEO}I^{PEO}(Q) + (1 - \phi^{PEO})I^{other}(Q)$, with other = PMMA or NPs].

The absence of side groups in PEO allows a straightforward interpretation of the unique peak centered at about 1.37 Å^{-1} as due to inter-main chain correlations with associated average distances of about $d_{chain} = 2\pi/Q_{max} \approx 4.6$ Å. The contributions to the structure factor of PMMA were investigated by molecular dynamics simulations[60] showing that the peak corresponding to inter-main chain distances $d_{chain} \approx 8.6$ Å is located at about 0.7 Å^{-1}, i.e., at lower Q values than the main peak. The patterns become even more complex for the nanoparticles. They do not appreciably change with deuteration and clearly differ from that of PMMA, showing a main maximum at about 1.15 Å^{-1} and a kind of shoulder around 0.90 Å^{-1}. We can argue that the differences with respect to bulk PMMA could be attributed to the contributions from the AEMA monomers, but deciphering the correlations leading to these features would require the help of molecular dynamics simulations and is beyond the scope of this work. Our aim here is to use these results to—at least qualitatively—address the question whether the short-range order in the mixtures reveals interpenetration of the components. If so, we would expect contributions of cross-correlation terms involving pairs of atoms of PEO and the other component to the structure factor of the mixtures in the Q range investigated. This implies that the measured structure factors would clearly differ from the simply weighed addition of the individual structure factors corresponding to the pure components. The result of such a combination is represented by the solid lines in Figure 3. The structure factor of the linear blend (Figure 3a) shows clear differences with respect to the simply added weighed patterns. On the other extreme, the *d*PEO/*h*NPs mixture results are rather close to the added patterns (Figure 3c); the *h*PEO/*d*NPs system shows qualitative agreement with the simple combination (Figure 3b), but the coincidence is not as clear as in the oppositely labeled sample. Thus, these WAXS results would suggest that the impact of PEO in the short-range order of PMMA in the blend is higher than in the mixture with the nanoparticles, and it seems to affect more the local structure in the *h*PEO/*d*NPs than in the *d*PEO/*h*NPs system. These conclusions would be in agreement with those obtained from the calorimetric study. Then, these structural results would also support the picture of a "true" nanocomposite for the system composed of NPs and PEO, where PEO chains surround the nanoparticles but do not deeply penetrate them. The confirmation of this result would need the input of small-angle neutron scattering (SANS) experiments in the labeled samples, which shall be subject of future work.

We have also followed the temperature dependence of the main structure factor peak of the linear blend and the nanocomposite *h*PEO/*d*NPs. The parameters characterizing this peak—position Q_{max} and width (full width at half-maximum fwhm)—are displayed in Figure 4. The change in their temperature dependencies is attributable to the occurrence of the main glass transition—corresponding to the majority component, the slow one, in both cases—which leads to changes in the expansion coefficient and correlation length.[61] Though the absolute values of Q_{max} and width differ from one sample to the other, their behavior reveal, within the uncertainties, practically the same value of the main glass-transition temperature (around 330 K), in excellent agreement with the results obtained by calorimetric experiments.

C. PMMA Dynamics in the NP's: α-Methyl Group Rotations. Figure 5 shows the QENS results on the *d*PEO/*h*NPs sample for selected temperatures and Q values. The data from the three instruments have been combined so as to cover ca. 3 decades in time. In this sample the signal is dominated by the incoherent contribution from the hydrogens in the NPs, ≈90% (see section A of the Supporting Information). Analogous to the observation in a nanocomposite with high content of PEO (25 wt %NPs) recently investigated by us,[62] we expect the dynamics in the time scale of QENS for PMMA in the NP's to be mainly the rotations of the α-methyl groups. The *d*PEO/*h*NPs data were thus described in the framework of the rotational rate distribution model[63−65] (see section B of the Supporting Information) usually applied for this kind of process in amorphous systems. This model introduces disorder through an distribution of rotational barriers. As can be seen in Figure 5, the data were successfully described under these assumptions. The two parameters of this model, σ and τ_0^{MG}—width and average value of the distribution of characteristic times for classical hopping, respectively (see section B of the Supporting Information)—were determined from these fits as a function of temperature. They are plotted in Figure 6. Within the uncertainties, the widths

dx.doi.org/10.1021/ma500215f | *Macromolecules* 2014, 47, 3005−3016

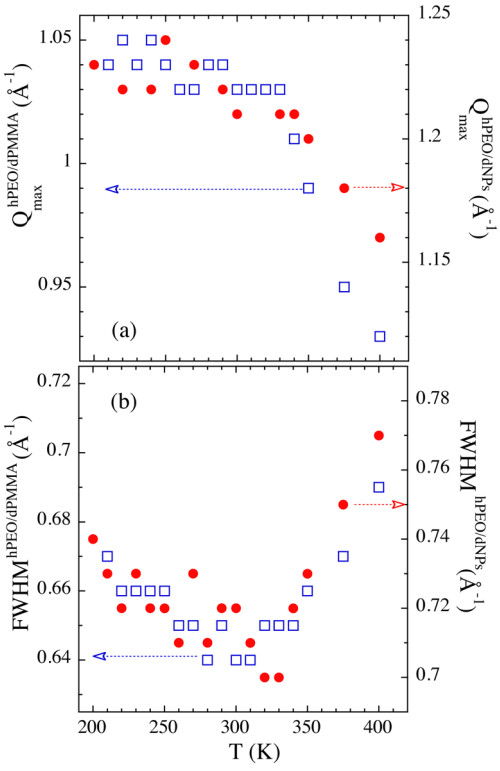

Figure 4. Temperature dependence of the position (a) and width (full width at half-maximum, fwhm) (b) of the main peak of the static structure factor of the blend *h*PEO/*d*PMMA (empty squares) and the *h*PEO/*d*NPs nanocomposite (filled circles).

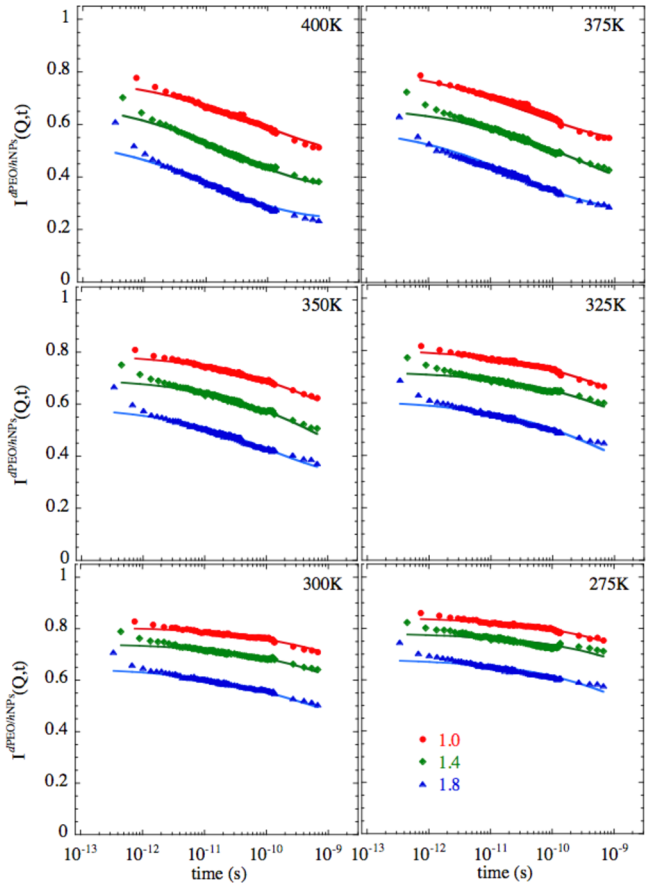

Figure 5. Fourier transformed and deconvoluted neutron scattering data of the *d*PEO/*h*NPs sample at different temperatures and the indicated values of Q (Å^{-1}). Solid lines are fitting curves considering α-MG rotation as the main process above ≈2 ps.

σ follow the expected temperature dependence $\sigma = (\sigma_E \log(e))/K_B T$ [solid line in Figure 6a], yielding a width for activation energies σ_E of 60 meV. For comparison, we have also plotted that for bulk PMMA (dashed-dotted line), whose distribution is narrower ($\sigma_E^{\text{bulk PMMA}}$ = 39 meV).[28] The broadening of the distribution of rotational barriers is likely a result of a more heterogeneous environment in the nanocomposite. On the one hand, we note the presence of the AEMA monomers and cross-linking units in the nanoparticle. On the other hand, the nanoparticles are mixed with PEO chains. In particular, we would expect the PMMA monomers at the interface with PEO to have a clearly different chemical environment from those in the inner part of the nanoparticle. For temperatures around and below the effective glass transition of the nanoparticles $T_{g,\text{eff}}^{NPs} \approx 346$ K (which coincides with the main glass transition of the system), the relaxation times τ_0^{MG} in the NPs follow an Arrhenius law with very similar average activation energy as that found in the bulk (solid line in Figure 6b, $\langle E_a^{MG} \rangle$ (bulk PMMA) = 290 meV). At the two highest temperatures investigated though the data tend to deviate from the bulk-like behavior, revealing faster times and a higher activation energy.

The question how α-methyl group rotation in PMMA is modified by blending was also addressed in the linear blend with the same PEO relative content (QENS experiments on a *d*PEO/*h*PMMA sample[28]). For such system, the α-MG dynamics in the neighborhood of the PMMA-effective glass transition was found to be rather insensitive to the presence of PEO, in a similar way as here observed in the nanocomposite. Conversely, for the nanocomposite with the opposite concentration recently investigated by us (75 wt % PEO/25 wt % PMMA-NPs),[62] the characteristic times for PMMA α-MG rotation were found to be smaller than the expectation from the bulk. All results corresponded to temperatures above the effective glass transition of the NPs. It was argued that the softening of the NPs could lead to a faster MG dynamics than that extrapolated from the glassy state. Such an explanation could also apply in the case of our high-temperature results.

D. PEO Dynamics. QENS results on the samples with protonated PEO allow us accessing the dynamics of the PEO component in both the nanocomposite and the linear blend. The function revealed by the experiments is actually the incoherent scattering function of the hydrogens of PEO, $S_{inc}^{PEO}(Q,t)$. Unfortunately, the number of assumptions involved in the modelization of the data (see section A of the Supporting Information) and the limited dynamic window accessible by QENS (even combining the three instruments here employed) prevent an unbiased and univocal determination of the functional form of this function. Therefore, we have made use of the information provided by fully atomistic MD simulations on the blend of linear chains PEO/PMMA of similar composition as that here investigated, which was reported in ref 41. In that work, $S_{inc}^{PEO}(Q,t)$ was parametrized in terms of Kohlrausch–Williams–Watts (KWW) functions

$$S_{inc}^{PEO}(Q,t) \approx e^{-(t/\tau)^{\beta}} \quad (1)$$

Here β is the shape parameter accounting for the deviations from a single-exponential function and τ is a Q- and T-dependent characteristic time. The values of the shape parameter β obtained

dx.doi.org/10.1021/ma500215f | *Macromolecules* 2014, 47, 3005–3016

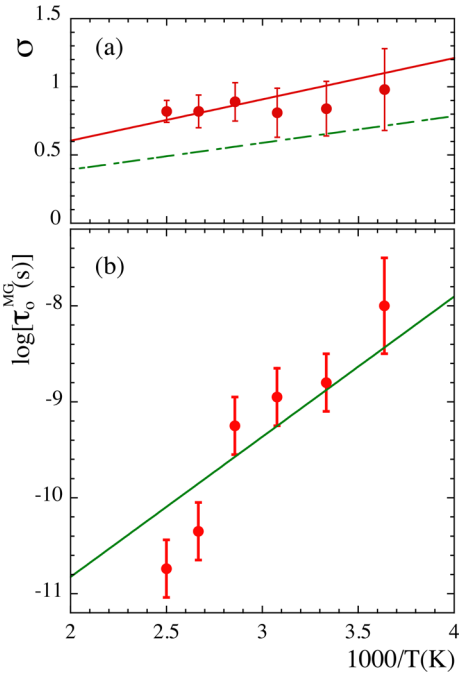

Figure 6. Inverse-temperature dependence of the width σ (a) and characteristic time (b) of the log−Gaussian distributions of rotation times for α-MGs in the PMMA-NPs in the nanocomposite (solid circles). In (a), the solid line is a fit to $\sigma = (\sigma_E \log(e))/K_B T$, and the dashed-dotted line shows the result for bulk PMMA.[28] Solid line in (b) is an Arrhenius fit with the same activation energy as that reported for bulk PMMA.

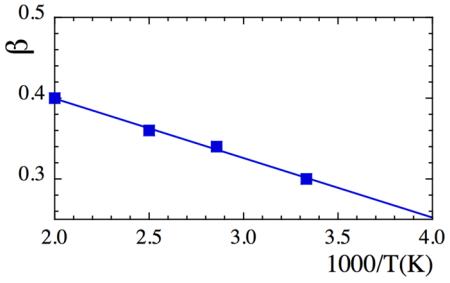

Figure 7. Inverse-temperature dependence of the shape parameter β deduced from MD simulations (filled squares)[41] for the KWW description of the intermediate incoherent scattering function of PEO in a PMMA/PEO blend. The linear fit shown by the solid line has been used to fix the β values in this work.

for the different temperatures simulated are displayed in Figure 7. They continuously decrease with decreasing temperature and can be well parametrized by the law $\beta = 0.547 - 73.7/T$ [K] (solid line in the figure).

We used these β-values (or their extrapolation) to describe $S_{inc}^{PEO}(Q,t)$ for PEO in both the nanocomposite with NPs and in the blend with linear chains. Figures 8 and 9 show the obtained fitting curves (see section A of the Supporting Information for the complete expressions used in each case). They reproduce very well all the experimental results above 2 ps, giving support to the choice of the shape parameter on the basis of the MD-simulation results.

Because of the variation of the shape parameter with temperature, in the following we will discuss the results obtained for the characteristic time in terms of the average time $\langle\tau\rangle$, which in the case of KWW functions is related with the parameter τ in

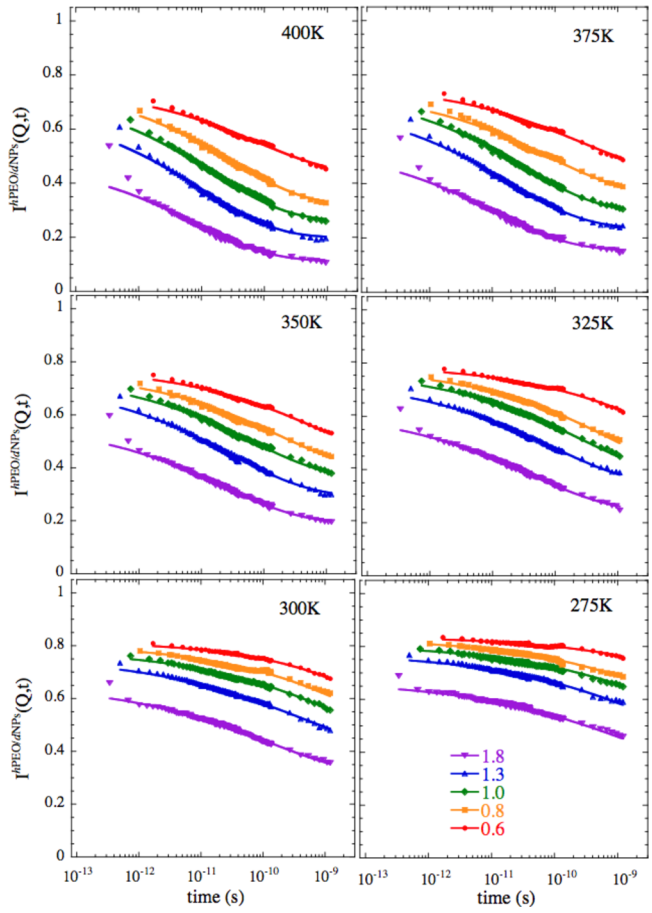

Figure 8. Fourier transformed and deconvoluted neutron scattering data of the *h*PEO/*d*NPs (nanocomposite) sample at different temperatures and the indicated values of Q (Å^{-1}). Solid lines are fitting curves considering a KWW functional form for the intermediate scattering function of the PEO component (see text).

eq 1 through the expression $\langle\tau\rangle = \tau\Gamma(1/\beta)/\beta$. Let us first consider the temperature dependence of the characteristic times at a representative Q value. This is shown in the Arrhenius representation of Figure 10b, which compiles the average characteristic times obtained by QENS at $Q = 1$ Å^{-1} for bulk PEO[28] and PEO in the two systems investigated in this work. We have chosen $Q = 1$ Å^{-1} because it is approximately at this Q value where the QENS characteristic times usually match those determined by other spectroscopic techniques like dielectric spectroscopy.[66,67] As can be seen in Figure 10b, this is also the case of bulk PEO when NMR data[12] (inverted empty triangles) are considered. Mixing PEO with a slower component slows down its dynamics (about 100-fold longer characteristic times than in the bulk, in the temperature range above the melting point where bulk data are available). We first concentrate on PEO in the nanocomposite. From the calorimetric measurements (reproduced again in Figure 10a) we have deduced a value of $T_{g,eff}^{hPEO} = 253$ K. This implies that the characteristic time of segmental dynamics of PEO in the nanocomposite should be of about 100 s in such temperature range. We have thus fitted the Williams−Landel−Ferry (WLF) expression

$$\log \tau(T) = \log \tau(T_{g,eff}^{hPEO}) - \frac{C_1(T - T_{g,eff}^{hPEO})}{C_2 + (T - T_{g,eff}^{hPEO})} \quad (2)$$

dx.doi.org/10.1021/ma500215f | *Macromolecules* 2014, 47, 3005−3016

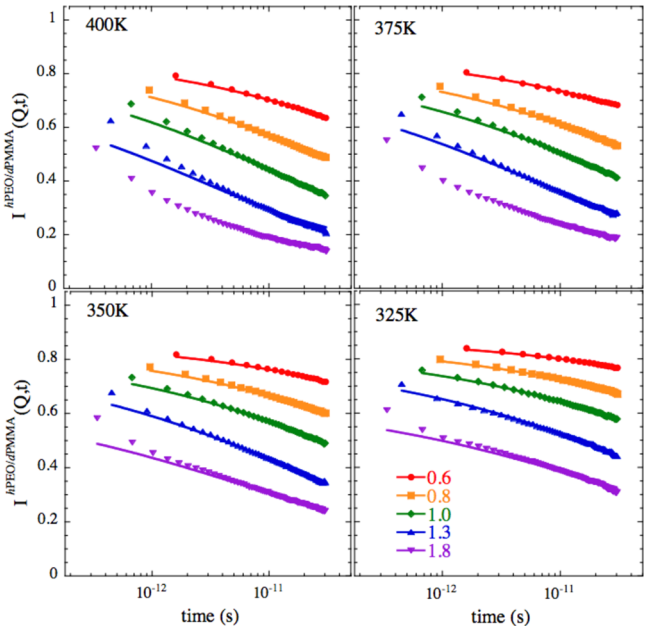

Figure 9. Fourier transformed and deconvoluted neutron scattering data of the *h*PEO/*d*PMMA (linear blend) sample at different temperatures and the indicated values of Q (Å^{-1}). Solid lines are fitting curves considering a KWW functional form for the intermediate scattering function of the PEO component (see the text). At 400 and 375 K the decay above ≈2 ps is just a small tail which cannot be properly modeled by KWW functions with realistic prefactors.

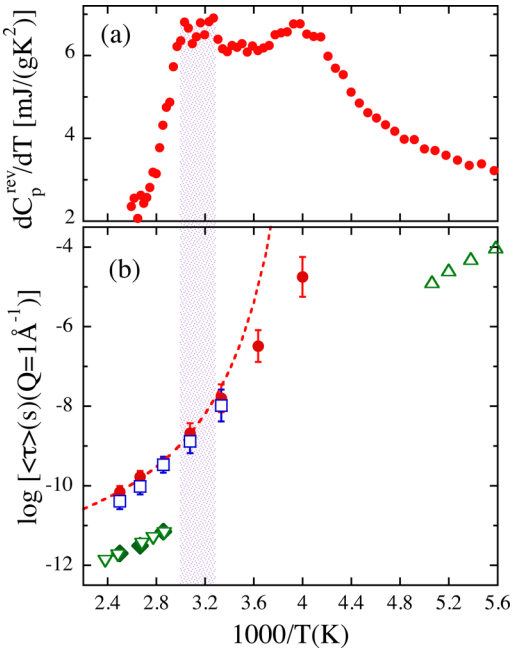

Figure 10. Inverse-temperature dependence of (a) the DSC data for *h*PEO/*d*NPs sample and (b) the average characteristic times obtained by QENS at Q = 1 Å^{-1} for PEO in the nanocomposite (filled circles), PEO in the blend with linear PMMA (empty squares), and bulk PEO (filled diamonds). For bulk PEO, NMR results[12] (inverted empty triangles) and dielectric data on the γ-process[69] (empty triangles) are also shown in (b). The shadowed area marks the effective glass-transition temperature region of the nanoparticles in the nanocomposite as determined from DSC. Dotted line is a WLF law describing the behavior of the characteristic time of segmental motions of PEO in the nanocomposite (see text).

to the high-temperature QENS data imposing this condition, $\tau(T_{g,eff}^{hPEO} = 253\ K) = 100$ s. The resulting curve (corresponding to $C_1 = 13.9$ and $C_2 = 21.9$ K) is the dotted line in Figure 10b. As can be seen, the temperature dependence displayed by the QENS characteristic times at low temperatures does not follow this law. The deviations take place at temperatures below the range corresponding to the effective glass transition of the nanoparticles (dashed area in the figure). Thus, at temperatures below $T_{g,eff}^{dNPs}$, from calorimetry we deduce the freezing of the PEO component with characteristic times of ≈ seconds around 250 K while simultaneously QENS reveal dynamics in the microseconds scale for $Q \approx 1$ Å^{-1} (length scales of the order of some angstroms). These observations strongly suggest a situation of confinement for PEO originated by the freezing of the other component. The results can be interpreted invoking the coexistence of dramatically slowing down PEO segments (following the vitrification approaching $T_{g,eff}^{hPEO}$) and rapidly moving PEO segments, which motions should be of localized nature in a rigid environment imposed by the slow component. Experimental evidences for a similar scenario have been recently proposed for the blend poly(vinyl methyl ether)/polystyrene.[68] As mentioned in the Introduction, this kind of interpretation was also proposed for the PEO/PMMA, PEO/PVAc, and PEO/PES blends.[28,55,57] Some other authors have identified this process with the Johari−Goldstein relaxation.[46] Whether this dynamics is referred to as Johari−Goldstein or confined process might ultimately be a semantic question. The results on PEO in the linear blend *h*PEO/*d*PMMA display very much the same behavior as those in the nanocomposite (see Figure 10b). Thus, the confinement effects induced by the freezing of the slow component in the system seem to be very similar in both cases. We note that the effective glass transition of linear PMMA in the blend *h*PEO/*d*PMMA and that of the *d*NPs in the *h*PEO/*d*NPs mixture are very much the same, which rationalizes this result. We can also see from Figure 10b that the confined dynamics of PEO at low temperature would be difficult to identify with that of secondary relaxations as taking place in the bulk. Looking now in detail in the high-temperature data, a slight difference could be envisaged between the results in both systems: in the nanocomposite, the temperature dependence of PEO dynamics seems to be slightly weaker than in the blend.

Now let us analyze the Q dependence of the characteristic times—a unique information provided by QENS spatial resolution. This is shown for the different temperatures investigated in Figure 11a for PEO in the nanocomposite and in Figure 11b for PEO in the linear blend. First we consider low-Q range ($Q \leq 0.8$ Å^{-1} approximately). In both kinds of environments the behavior of $\langle\tau\rangle$ is qualitatively the same; it follows a power-law in Q

$$\langle\tau\rangle = a(T)Q^{-x} \qquad (3)$$

(see solid lines in the figures), and at higher Q values it tends to deviate from such a law, becoming larger. The values of the x-exponent in eq 3 are displayed in Figure 12. For temperatures $T \leq 350$ K they are, within the uncertainties, identical for both kinds of environments. At the two highest temperatures investigated though, the x-parameter corresponding to the nanocomposite tends to dramatically decrease with increasing temperature and becomes smaller values than those found for the linear blend.

Considering explicitly the Q dependence of the characteristic times (eq 3) in the intermediate scattering function of PEO (eq 1), we obtain

dx.doi.org/10.1021/ma500215f | *Macromolecules* 2014, 47, 3005−3016

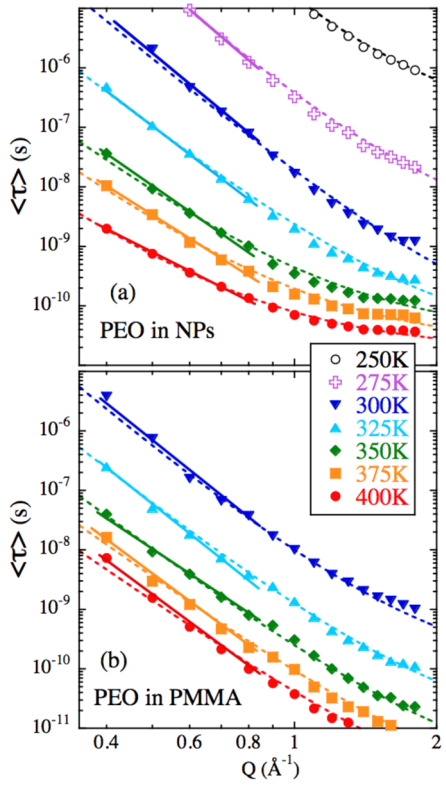

Figure 11. Momentum transfer dependence of the average characteristic times for PEO dynamics in the nanocomposite (a) and in the linear blend (b) at the temperatures indicated. The solid lines are power laws $\langle\tau\rangle \propto Q^{-x}$ describing the low-Q behavior. Dotted lines are fits of the anomalous jump diffusion model (eq 6).

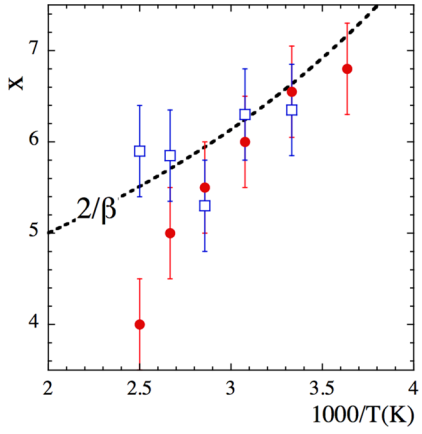

Figure 12. Inverse-temperature dependence of the exponent x characterizing the Q dependence of the average characteristic times for PEO dynamics in the nanocomposite (filled circles) and in the blend with linear PMMA chains (empty squares) for approximately $Q \leq 0.8$ Å^{-1}. Dotted line displays the Gaussian prediction $x = 2/\beta$.

$$S_{\mathrm{inc}}^{\mathrm{PEO}}(Q,t) \approx \mathrm{e}^{-a(T)^{-\beta}Q^{x\beta}t^{\beta}} \tag{4}$$

If $x\beta = 2$, this expression corresponds to a Gaussian function in the Q variable $[\mathrm{e}^{-\langle r^2(t)\rangle Q^2/6}]$. Then, the mean-squared displacement of the hydrogens would be directly obtained as $\langle r^2(t)\rangle \propto t^{\beta}$; i.e., the atoms undergo sublinear diffusion. The condition for Gaussian behavior $x = 2/\beta$ is represented by the dotted line in Figure 12. The results obtained for PEO in the linear blend fulfill, within the uncertainties, the Gaussian approximation in the whole temperature range investigated. This finding fully agrees with the MD simulations results of ref 41. From the simulated atomic trajectories it is namely possible to quantify the deviations from Gaussian behavior through the calculation of the non-Gaussian parameter α_2 ($\alpha_2 = 0$ in the Gaussian case). This parameter turned out to present very small values for PEO in the blend. Accordingly, after the decaging regime ($t > 30$ ps approximately), the mean-squared displacement of PEO's hydrogens in the simulated blend was found to increase sublinearly with time as $\langle r^2(t)\rangle \propto t^{y}$ with $y \approx \beta$. Our experimental results thus provide an additional source of validation for those MD simulations.

For PEO in the NPs, the exponents found in the low-Q range also indicate close to Gaussian behavior in the temperature range $T \leq 350$ K. However, for the two highest temperatures they clearly deviate from the Gaussian prediction. We will discuss this result later.

As pointed out above, in the high-Q range investigated the Q dependence of the characteristic times tends to deviate from the asymptotic low-Q power law (eq 3) for PEO in both systems and all the temperatures investigated. These deviations consist of a kind of flattening of $\langle\tau\rangle$. They occur in a rather similar way for both samples for 325 and 300 K, but at higher temperatures they become more pronounced for PEO in the nanocomposite.

Deviations from the Gaussian behavior ($\tau \propto Q^{-2/\beta}$) can be rationalized invoking the temporary localization of the microscopic motions underlying the sublinear diffusion. For simple diffusion, this ingredient is captured by the jump diffusion model.[70−72] In this model, an atom remains in a given site for a time τ_0, where it vibrates around a center of equilibrium. After τ_0, it moves rapidly to a new position. These jumps are assumed to be randomly orientated and their moduli l are distributed according to a function

$$f_0(l) = \frac{l}{{l_0}^2}\mathrm{e}^{(-l/l_0)} \tag{5}$$

The parameter l_0 is the preferred jump distance. This model was generalized for the case of subdiffusive motions—which are those usually observed in glass-forming systems, in particular in polymers—by the anomalous jump diffusion (AJD) model.[73,74] The intermediate scattering function in the AJD model is a stretched exponential (eq 1) where the characteristic time follows the law

$$\tau^{\mathrm{AJD}} = \tau_0\left(1 + \frac{1}{{l_0}^2Q^2}\right)^{1/\beta} \tag{6}$$

with $\tau_0(l_0Q)^{-2/\beta}$ and τ_0 as asymptotic low-Q and high-Q limits, respectively. In the AJD model, at large length scales/long times the resulting mean-squared displacement asymptotically follows a sublinear increase with time

$$\langle r^2(t)\rangle = 6{l_0}^2(t/\tau_0)^{\beta} \tag{7}$$

The AJD model has been successfully applied to a number of polymers,[67,73−78] including bulk PEO.[62] Figure 11 shows that this model also provides very good descriptions (dotted lines) of the experimentally obtained characteristic times for PEO in the blend and in the nanocomposite.

Figure 13 presents the temperature dependence of the average elementary time $\langle\tau_0\rangle = \tau_0\Gamma(1/\beta)/\beta$ and the preferred jump distance l_0 obtained from these fits. We first discuss the results in the temperature range below the effective glass-transition

dx.doi.org/10.1021/ma500215f | Macromolecules 2014, 47, 3005−3016

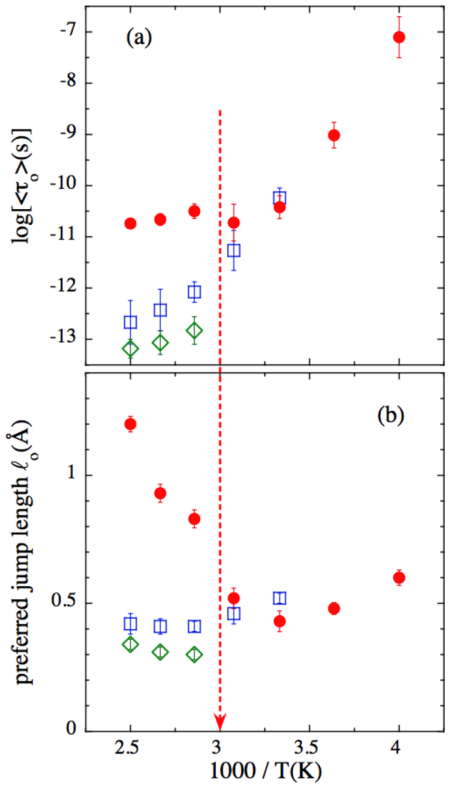

Figure 13. Inverse-temperature dependence of the parameters involved in the description of the characteristic times of bulk PEO (empty diamonds) and PEO in the nanocomposite (filled circles) and in the linear blend (empty squares) in terms of the anomalous jump diffusion model: average residence time (a); preferred jump distance (b). The arrow marks the main glass-transition temperature of the mixtures.

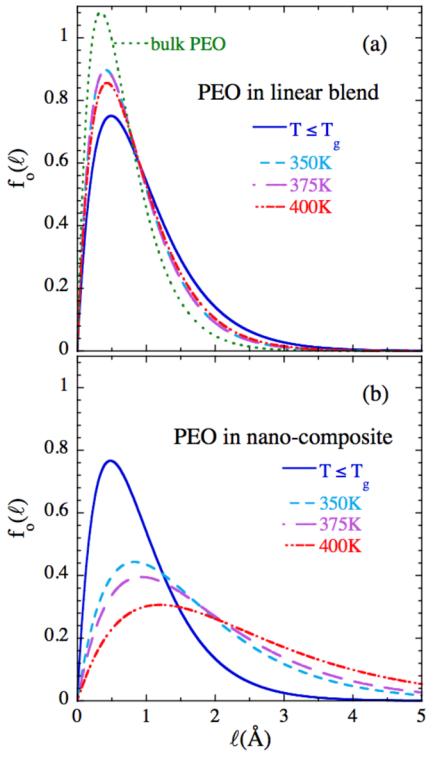

Figure 14. Distribution function of elementary jump distances in the AJD model description of PEO results in the blend with linear PMMA chains (a) and in the nanocomposite (b) at different temperatures. The solid lines correspond to the average value of l_0 observed in the glassy state (0.48 and 0.49 Å, respectively). In (a) the distribution function deduced for bulk PEO at 400 K is shown for comparison.

temperature of the slow component $T_{g,eff}^{PMMA} = 326$ K, $T_{g,eff}^{NPs} = 327$ K (which coincides with the main glass-transition of the system). In this regime the values of the parameters are, within the uncertainties, practically the same for both systems. This means that the dynamics of PEO in a frozen environment is independent of the topology of the PMMA component (as linear chains or in the form of nanoparticles). In this regime, the characteristic time $\langle\tau_0\rangle$ increases dramatically with decreasing temperature, suggesting a rapid enhancement of the localization of the motions giving rise to the later sublinear diffusion. The preferred jump length is, within the errors, independent of temperature and system, and amounts to $\langle l_0\rangle_{T\le T_{g,eff}^{PMMA}} \approx 0.5$ Å.

We now focus on temperatures above $T_{g,eff}^{PMMA} = 326$ K, $T_{g,eff}^{NPs} = 327$ K. In this regime, the local dynamics of PEO differs in both samples. In the blend, the average residence times become faster with increasing temperature, and the distances involved in the elementary jumps for sublinear diffusion do not sensitively vary. On the contrary, in the nanocomposite we observe that the value of the elementary time remains approximately the same as at the glass transition and the preferred jump length drastically increases with increasing temperature. In this temperature range we can compare the results with the corresponding ones for bulk PEO—there are available data above its melting point. With respect to the bulk, in the blend the motions of PEO at local length scales are somewhat less Gaussian: the value of the preferred jump length is slightly larger and consequently the distribution of jump lengths a little bit broader (see Figure 14a); moreover, the residence time is 3−5-fold longer. The vicinity of PMMA mobile—but slower—chain segments thus induces an additional source for distributed environments and slows down the PEO local dynamics. Nevertheless, the behavior displayed by PEO in the blend is qualitatively the typical one observed for glass-forming polymers in equilibrium,[67,73−78] and these results could perfectly be rationalized in the light of the existing knowledge on polymer blend dynamics, invoking the concepts of dynamic heterogeneity and concentration fluctuations.[6] This was also the situation reported from the QENS studies of the minority PEO component in blends with PVAc[55] and PES,[57] but this is clearly not the case for PEO in the nanocomposite. The values of the average residence times $\langle\tau_0\rangle$ are extremely long—more than 100-fold longer than in bulk. We note that these times are directly related with the decaging processes and in the supercooled liquid (metastable) equilibrium regime are expected to be located typically in the picosecond region. Thus, these results suggest that in the nanocomposite PEO segments are momentarily highly efficiently trapped by the PMMA nanoparticles—even at temperatures where the latter are above their glass-transition temperature. The "effective cage" imposed to a PEO hydrogen in a PMMA-NPs-rich environment takes an extremely long time to "soften". However, once PEO segments get rid of this cage, the jumps can be relatively large with respect to those taking place in the PEO or linear PMMA chains environments, as can be seen in the distributions of jump lengths depicted in Figure 14. With increasing temperature, the extent of the local motions becomes larger on average, leading to larger values of the resulting mean-squared displacements (eq 7). Simultaneously, the broader and broader distributions of

dx.doi.org/10.1021/ma500215f | Macromolecules 2014, 47, 3005−3016

relatively long elementary jump lengths lead to larger deviations from Gaussian behavior of PEO motions, as manifested in the value of the x-exponent in eq 3 (Figure 12).

Once the PMMA component starts to be mobile, its topology seems thus to be a determining ingredient in the dynamics of PEO segments. The presence of linkages between PMMA monomers causes the temporary blockage of the more flexible component and, when the latter can leave such an imposed cage, it jumps over larger distances as those characteristic for the motions either in bulk or in an environment of linear PMMA chains. In this trapping mechanism the local loops in the nanoparticles may play an important role. As it has been shown by MD simulations[79] and is schematically illustrated in Figure 1, a relatively large number of the cross-links occur between nearest monomers (or monomers very close in real space). These bonds do not contribute to the collapse of the macromolecule into a globular structure—this is controlled by cross-links involving monomers separated by large contour distances—but it could be expected that they would strongly restrict the local motions of the PMMA portions involved in the loops with respect to those in a linear macromolecule. The local relaxation of the such affected PMMA segments would be severely obstructed, and if they are at the interface with PEO, this might greatly hamper the development of PEO's motions.

IV. SUMMARY AND CONCLUSIONS

The weak sensitivity of the glass transition of the nanoparticles upon mixing with PEO chains and the small contributions of PEO/NPs cross-correlations to the static structure factor of the mixture suggests no significant penetration of PEO chains in the soft nanoparticles. This qualifies the PEO/NPs mixture investigated as a "true" nanocomposite. Quasielastic neutron scattering on labeled samples has allowed the characterization of individual component dynamics in such a nanocomposite. The α-methyl group dynamics of PMMA—the main process accessed in the investigated temperature/time window—is hardly affected by the presence of PEO, with the exception of showing a somewhat broader distribution of potential barriers with respect to bulk PMMA. This could be attributed to markedly different environments for methyl groups in the nanoparticles, depending on their location either close to the interface with PEO or deep within the NP. Another possible source of heterogeneous environments would be the presence of AEMA monomers and cross-linking units in the nanoparticle. The investigation of the PEO component has been performed considering the equivalent blend of linear chains as reference. In the vicinity of its effective glass transition in the nanocomposite, QENS reveals average characteristic times of PEO at $Q = 1$ Å^{-1} which are in the microseconds range. This observation can be considered as a proof for the occurrence of confined dynamics of PEO in the nanocomposite below the effective glass-transition temperature of the slow component—the NPs. Moreover, the freezing of the PMMA-based component leads to a dynamical response of PEO which shows the same features independently of the topology of the former. This finding supports the interpretation of the motions of the fast PEO component as confined by a surrounding rigid matrix. Interestingly enough, the differences in PEO dynamics emerge above the effective glass transition of the slow component, when the surrounding environment of PEO starts to be mobile. There, both the blend and the nanocomposite are in the supercooled liquid (metastable) equilibrium state. Linear PMMA motions are enough to allow PEO segments to move in a way typical of supercooled polymers in metastable equilibrium, but the presence of PMMA leads to more distributed environments and moderately slows it down. Contrarily, PEO dynamics in the nanocomposite develops larger and larger deviations from Gaussian behavior as the mobility of the nanoparticles increases. These enhanced deviations are caused by an increase of the spatial extent of the elementary jumps of PEO for segmental dynamics with increasing temperature. These jumps appear to be very heterogeneous and only take place after the segment has been trapped for a very long time—more than 2 orders of magnitude longer than in bulk or surrounded by linear PMMA chains—in effective cages imposed by the nanoparticles. We speculate that in this trapping mechanism the local loops in the nanoparticles—particularly those affecting the segments at the surface—may play an important role.

■ ASSOCIATED CONTENT

Supporting Information

Neutron scattering data evaluation. This material is available free of charge via the Internet at http://pubs.acs.org.

■ AUTHOR INFORMATION

Corresponding Author

*E-mail: a.arbe@ehu.es (A.A.).

Notes

The authors declare no competing financial interest.

■ ACKNOWLEDGMENTS

Isabel Asenjo and Lorea Buruaga are gratefully acknowledged for assistance during sample preparation and Yixi Su for helping us with the DNS measurements. We thank support by the projects IT-654-13 (GV) and MAT2012-31088. This work is based on experiments performed at the FOCUS instrument operated by the Swiss spallation neutron source SINQ, Paul Scherrer Institute, Villigen, Switzerland, and at the SPHERES and DNS instruments operated by JCNS at the Forschungs-Neutronenquelle Heinz Maier-Leibnitz (FRM II), Garching, Germany, and has been supported by the European Commission under the seventh Framework Programme through the "Research Infrastructures" action of the "Capacities" Programme, NMI3-II Grant No. 283883.

■ REFERENCES

(1) Mackay, M. E.; Dao, T. T.; Tuteja, A.; Ho, D. L.; van Horn, B.; Kim, H.-C.; Hawker, C. J. *Nat. Mater.* **2003**, *2*, 762.
(2) Oria, L.; Aguado, R.; Pomposo, J. A.; Colmenero, J. *Adv. Mater.* **2010**, *22*, 3038.
(3) Gillissen, M. A. J.; Voets, I. K.; Meijer, E. W.; Palmans, A. R. A. *Polym. Chem.* **2012**, *3*, 3166.
(4) Krishnan, R. S.; Mackay, M. E.; Duxbury, P. M.; Pastor, A.; Hawker, C. J.; Van Horn, B.; Asokan, S.; Wong, M. S. *Nano Lett.* **2007**, *7*, 484.
(5) Krishnan, R. S.; Mackay, M. E.; Hawker, C. J.; Van Horn, B. *Langmuir* **2005**, *21*, 5770.
(6) Colmenero, J.; Arbe, A. *Soft Matter* **2007**, *3*, 1474.
(7) Maranas, J. K. *Curr. Opin. Colloidal Interface Sci.* **2007**, *12*, 29.
(8) Colby, R. H. *Polymer* **1989**, *30*, 1275.
(9) Xia, J. L.; Wang, C. H. *J. Chem. Phys.* **1991**, *94*, 3229.
(10) Brosseau, C.; Guillermo, A.; Cohen-Addad, J. P. *Macromolecules* **1992**, *25*, 4535.
(11) Zawada, J. A.; Ylitalo, C. M.; Fuller, G. G.; Colby, R. H.; Lodge, T. P. *Macromolecules* **1992**, *25*, 2896.
(12) Lartigue, C.; Guillermo, A.; Cohen-Addad, J. P. *J. Polym. Sci., Part B: Polym. Phys.* **1997**, *35*, 1095.
(13) Schantz, S. *Macromolecules* **1997**, *30*, 1419.
(14) Wästlund, C.; Maurer, F. H. J. *Macromolecules* **1997**, *30*, 5870.

(15) Schmidt, M.; Maurer, F. H. J. *J. Polym. Sci., Part B: Polym. Phys.* **1998**, *36*, 1061.
(16) Guillermo, A.; Lartigue, C.; Cohen Addad, J. P. *Macromolecules* **1998**, *31*, 769.
(17) Vernela, J.; Rychwalskia, R. W.; Pelsek, V. *Thermochim. Acta* **1999**, *342*, 115.
(18) Dionísio, M.; Fernandes, A. C.; Mano, J. F.; Correia, N. T.; Sousa, R. C. *Macromolecules* **2000**, *33*, 1002.
(19) Silva, G. G.; Machado, J. C.; Song, M.; Hourston, D. J. *J. Appl. Polym. Sci.* **2000**, *77*, 2034.
(20) Lutz, T. R.; He, Y.; Ediger, M. D.; Cao, H.; Lin, G.; Jones, A. A. *Macromolecules* **2003**, *36*, 1724.
(21) Diniz, T. M. F. F.; Tavares, M. I. B. *J. Appl. Polym. Sci.* **2003**, *90*, 2955.
(22) Ngai, K. L.; Roland, C. M. *Macromolecules* **2004**, *37*, 2817.
(23) Jin, X.; Zhang, S.; Runt, J. *Macromolecules* **2004**, *37*, 8110.
(24) García Sakai, V.; Chen, C.; Maranas, J. K.; Chowdhuri, Z. *Macromolecules* **2004**, *37*, 9975.
(25) Cao, H.; Lin, G.; Jones, A. A. *J. Polym. Sci., Part B: Polym. Phys.* **2005**, *43*, 2433.
(26) García Sakai, V.; Maranas, J. K.; Chowdhuri, Z.; Peral, I.; Copley, J. R. D. *J. Polym. Sci., Part B: Polym. Phys.* **2005**, *43*, 2914.
(27) Farago, B.; Chen, C.; Maranas, J. K.; Kamath, S.; Colby, R. H.; Pasquale, A. J.; Long, T. E. *Phys. Rev. E* **2005**, *72*, 031809.
(28) Genix, A.-C.; Arbe, A.; Alvarez, F.; Colmenero, J.; Willner, L.; Richter, D. *Phys. Rev. E* **2005**, *72*, 031808.
(29) Haley, J. C.; Lodge, T. P. *J. Chem. Phys.* **2005**, *122*, 234914.
(30) Liu, J.; Sakai, V. G.; Maranas, J. K. *Macromolecules* **2006**, *39*, 2866.
(31) Lodge, T. P.; Wood, E. R.; Haley, J. C. *J. Polym. Sci., Part B: Polym. Phys.* **2006**, *44*, 756.
(32) Niedzwiedz, M.; Wischnewski, A.; Monkenbusch, M.; Richter, D.; Genix, A. C.; Arbe, A.; Colmenero, J.; Strauch, M.; Straube, E. *Phys. Rev. Lett.* **2007**, *98*, 168301.
(33) Wu, X.; Shang, S.; Xu, Q.; Liu, C.; Zhu, Z. *Appl. Phys. Lett.* **2008**, *93*, 011910.
(34) García Sakai, V.; Maranas, J. K.; Peral, I.; Copley, J. R. D. *Macromolecules* **2008**, *41*, 3701.
(35) Gaikwad, A. N.; Wood, E. R.; Ngai, T.; Lodge, T. P. *Macromolecules* **2008**, *41*, 2502.
(36) Mpoukouvalas, K.; Floudas, G. *Macromolecules* **2008**, *41*, 1552.
(37) Zeroni, I.; Ozair, S.; Lodge, T. P. *Macromolecules* **2008**, *41*, 5033.
(38) Sacristan, J.; Chen, C.; Maranas, J. K. *Macromolecules* **2008**, *41*, 5466.
(39) Chen, C.; Maranas, J. K. *Macromolecules* **2009**, *42*, 2795.
(40) Shang, S. Y.; Fang, Z. P.; Zhu, Z. G. *Physica B: Condens. Matter* **2009**, *404*, 1200.
(41) Brodeck, M.; Alvarez, F.; Moreno, A. J.; Colmenero, J.; Richter, D. *Macromolecules* **2010**, *43*, 3036.
(42) Jeddi, K.; Qazvini, N. T.; Jafari, S. H.; Khonakdar, H. A. *J. Polym. Sci., Part B: Polym. Phys.* **2010**, *48*, 2065.
(43) Wu, X.; Liu, C.; Zhu, Z.; Ngai, K. L.; Wang, L.-M. *Macromolecules* **2011**, *44*, 3605.
(44) Didiens, D.; Brodeck, M.; Heuer, A. *Europhys. Lett.* **2011**, *95*, 56003.
(45) Mu, D.; Li, J.-Q.; Wang, S. *J. Appl. Polym. Sci.* **2011**, *122*, 64.
(46) Ngai, K. L.; Wang, L.-M. *J. Chem. Phys.* **2011**, *135*, 194902.
(47) Brodeck, M.; Alvarez, F.; Colmenero, J.; Richter, D. *Macromolecules* **2012**, *45*, 536.
(48) Shi, W.; Yang, J.; Zhang, Y.; Luo, J.; Liang, Y.; Han, C. C. *Macromolecules* **2012**, *45*, 941.
(49) Schwahn, D.; Pipich, V.; Richter, D. *Macromolecules* **2012**, *45*, 2035.
(50) Satoaki, K.; Pipich, V.; Masami, K. *J. Colloid Interface Sci.* **2012**, *384*, 87.
(51) Shi, W.; Xie, X.-M.; Han, C. C. *Macromolecules* **2012**, *45*, 8336.
(52) Evans, C. M.; Torkelson, J. M. *Polymer* **2012**, *53*, 6118.
(53) Colmenero, J. *Macromolecules* **2013**, *46*, 5363.
(54) Ngai, K. L.; Capaccioli, S. *J. Chem. Phys.* **2013**, *138*, 054903.
(55) Tyagi, M.; Arbe, A.; Alegría, J.; Colmenero, A.; Frick, B. *Macromolecules* **2007**, *40*, 4568.
(56) Urakawa, O.; Ujiia, T.; Adachi, K. *J. Non-Cryst. Solids* **2006**, *352*, 42.
(57) Genix, A.-C.; Arbe, A.; Arrese-Igor, S.; Colmenero, J.; Richter, D.; Frick, B.; Deen, P. P. *J. Chem. Phys.* **2008**, *128*, 184901.
(58) Sanchez-Sanchez, A.; Akbari, S.; Etxeberria, A.; Arbe, A.; Gasser, U.; Moreno, A. J.; Colmenero, J.; Pomposo, J. A. *ACS Macro. Lett.* **2013**, *2*, 491.
(59) Deuteration produces a slight increase of the value of the glass transition temperature in the nanoparticles. Differences of some degrees in T_g upon deuteration have already been reported in the literature (see, e.g., ref 80).
(60) Genix, A.-C.; Arbe, A.; Alvarez, F.; Colmenero, J.; Schweika, W.; Richter, D. *Macromolecules* **2006**, *39*, 3947.
(61) Frick, B.; Richter, D.; Ritter, C. *Europhys. Lett.* **1989**, *9*, 557.
(62) Bhowmik, D.; Pomposo, J. A.; Juranyi, F.; García-Sakai, V.; Zamponi, M.; Su, Y.; Arbe, A.; Colmenero, J. *Macromolecules* **2014**, *47*, 304.
(63) Chahid, A.; Alegría, A.; Colmenero, J. *Macromolecules* **1994**, *27*, 3282.
(64) Colmenero, J.; Mukhopadhyay, R.; Alegría, A.; Frick, B. *Phys. Rev. Lett.* **1998**, *80*, 2350.
(65) Colmenero, J.; Moreno, A.; Alegría, A. *Prog. Polym. Sci.* **2005**, *30*, 1147.
(66) Colmenero, J.; Arbe, A.; Alegría, A. *J. Non-Cryst. Solids* **1994**, *172*−*174*, 126.
(67) Capponi, S.; Arbe, A.; Cerveny, S.; Busselez, R.; Frick, B.; Embs, J.; Colmenero, J. *J. Chem. Phys.* **2011**, *134*, 204906.
(68) Plaza-García, S.; Lund, R.; Arbe, A.; Alegría, A.; Colmenero, J.; Quirk, R. P., in progress.
(69) Jin, X.; Zhang, S.; Runt, J. *Polymer* **2002**, *43*, 6247.
(70) Egelstaff, P. A., Ed.; *An Introduction to the Liquid State*; Oxford University Press: New York, 1992.
(71) Springer, T. *Quasielastic Neutron Scattering for the Investigation of Diffusive Motions in Solids and Liquids*; Springer Tracts in Modern Physics; Springer-Verlag: Berlin, 1972; Vol. *64*.
(72) Singwi, K. S.; Sjölander, A. *Phys. Rev.* **1960**, *119*, 863.
(73) Arbe, A.; Colmenero, J.; Alvarez, F.; Monkenbusch, M.; Richter, D.; Farago, B.; Frick, B. *Phys. Rev. Lett.* **2002**, *89*, 245701.
(74) Arbe, A.; Colmenero, J.; Alvarez, F.; Monkenbusch, M.; Richter, D.; Farago, B.; Frick, B. *Phys. Rev. E* **2003**, *67*, 051802.
(75) Colmenero, J.; Arbe, A.; Alvarez, F.; Narros, A.; Richter, D.; Monkenbusch, M.; Farago, B. *Pramana* **2004**, *63*, 25.
(76) Genix, A.-C.; Arbe, A.; Alvarez, F.; Colmenero, J.; Farago, B.; Wischnewski, A.; Richter, D. *Macromolecules* **2006**, *39*, 6260.
(77) Pérez Aparicio, R.; Arbe, A.; Colmenero, J.; Frick, B.; Willner, L.; Richter, D.; Fetters, L. J. *Macromolecules* **2006**, *39*, 1060.
(78) Colmenero, J.; Alvarez, F.; Khairy, Y.; Arbe, A. *J. Chem. Phys.* **2013**, *139*, 044906.
(79) Moreno, A. J.; Lo Verso, F.; Sanchez-Sanchez, A.; Arbe, A.; Colmenero, J.; Pomposo, J. A. *Macromolecules* **2013**, *46*, 9748−9759.
(80) Zorn, R.; Arbe, A.; Colmenero, J.; Frick, B.; Richter, D.; Buchenau, U. *Phys. Rev. E* **1995**, *52*, 781.